Application of the eigenstrain approach to predict the residual stress distribution in laser shock peened AA7050-T7451 samples

Coratella, S. , Sticchi, M. , Toparli, M.B. , Fitzpatrick, M.E. and Kashaev, K.

Original citation & hyperlink:
Coratella, S. , Sticchi, M. , Toparli, M.B. , Fitzpatrick, M.E. and Kashaev, K. (2015) Application of the eigenstrain approach to predict the residual stress distribution in laser shock peened AA7050-T7451 samples. Surface and Coatings Technology, volume 273 : 39-49.
http://dx.doi.org/10.1016/j.surfcoat.2015.03.026

Application of the eigenstrain approach to predict the residual stress distribution in laser shock peened AA7050-T7451 samples

S. Coratella[1,a], M. Sticchi[2], M.B. Toparli[3], M. E. Fitzpatrick[1], N. Kashaev[2]

[1]Faculty of Engineering and Computing, Coventry University, Priory Street, Coventry CV1 5FB, UK

[2]Helmholtz-Zentrum Geesthacht, Institute of Materials Research, Material Mechanics, Max-Planck-Straße 1, D-21502 Geesthacht, Germany

[3]Defense Industries Research and Development Institute, (TÜBITAK SAGE), P.K. 16, 06261, Mamak, Ankara, Turkey

[a]CoratelS@uni.coventry.ac.uk
Phone number: +44 (0) 7544821209

Keywords: Eigenstrain, Residual stress prediction, Laser Shock Peening, AA7050

Abstract

Laser Shock Peening allows the introduction of deep compressive residual stresses into metallic components. It is applicable to most metal alloys used for aerospace applications. The method is relatively expensive in application, and therefore development studies often rely heavily on Finite Element Modelling to simulate the entire process, with a high computational cost. A different approach has been used recently, the so-called eigenstrain approach. The present study looks at the feasibility of applying the eigenstrain method for prediction of the residual stress in a sample that contains curved surface features. The eigenstrain is determined from a simple geometry sample, and applied to the more complex geometry to predict the residual stress after Laser Shock Peening. In particular the prediction of residual stress at a curved edge, and for different values of material thickness, have been studied. The research has demonstrated that the eigenstrain approach gives promising results in predicting residual stresses when both the thickness and the geometry of the peened surface is altered.

1 Introduction

Laser Shock Peening (LSP) is a relatively new surface treatment technique which has been shown to improve fatigue life in several metal alloys including titanium alloy [1], steel [2] and several aluminium

alloys for aerospace applications like AA2024 [3] and AA7050 [4,5]. In LSP a pulsed high-energy laser beam is fired onto a sample surface that is covered by a transparent layer (usually water): an opaque ablative layer (such as thin aluminium tape, or paint) is also often applied. When the beam hits the sample surface, the opaque layer turns into vapour, and the laser energy increases both its temperature and pressure and generates a plasma. The plasma is confined between the water layer and the sample surface, generating shock waves that propagate into the sample. As the shock waves propagate into the material, a value of stress greater than the Hugoniot Elastic Limit value (HEL or Shock Yield Strength) is reached and the material deforms plastically at the surface. This permanent deformation generates surface compressive residual stresses [6] which greatly improve the fatigue life of a component as well as its corrosion behaviour [7].

One of the keys to understand and quantify the effects of LSP on fatigue life is a clear knowledge of the residual stress state. The Finite Element (FE) simulation technique is widely recognised as an effective tool to gain an understanding of the induced residual stress state and of the LSP process itself. It was first applied to the problem by Braisted and Brockman in 1999 [8] and, in the past decade, several researchers have simulated the laser-generated shock waves propagating into different metal materials through this method [9]. Although some of these simulations produce a close match with experimentally measured residual stresses, the process complexity and the high number of variables involved mean that each new application requires starting the modelling process from scratch. In particular, to simulate correctly the shock waves, it is critical to model the plasma pressure accurately, in terms of its magnitude as a function of time, in a way that correctly represents the physics of the process, for a given LSP treatment. Furthermore, in the FE method, the high-strain-rate deformations of the material under a shock impact are simulated with constitutive models that describe the material behaviour [10]. However, they may be hard to calibrate and involve a large number of parameters that are required to be determined from material tests. Additional difficulties in modelling the LSP process by the use of the FE approach could be encountered when dealing with complex geometries, owing to the high computational cost required for such simulations.

1.1 The Eigenstrain Approach

The eigenstrain approach to predict residual stresses has aroused considerable interest in recent years. This is due to the fact that it is possible to reconstruct the complete residual stress field of a component, starting with a set of residual stress measurements on a baseline sample, with reasonable computational time.

The term eigenstrain was suggested for the first time by Mura [11] and indicates any permanent or non-elastic strain generated inside a component after a non-elastic process. In the literature it is possible to find several terms indicating eigenstrain like inelastic strain [12], inherent strain [13] and equivalent transformation strain [14]. The eigenstrain term can incorporate creep strain, phase transformation strain, thermal strain and so on. These different non-elastic strain components cannot be separated and this

property is actually an advantage when we apply eigenstrain into an FE model. Although the eigenstrain approach is mathematically complicated and it is feasible only for simple geometry samples, with limited engineering application, as has been shown in [15,16], recently some interesting results from the application of eigenstrain prediction have been presented for applications such as friction stir welding [17], shot peening [18], and LSP [19]. All these results were completely or partially based on the model proposed by Korsunsky called Eigenstrain Reconstruction Method (ERM) and a complete analysis of the method can be found in [20]. With the ERM is possible to know the whole residual stress field within a body when only a bunch of measurements of them are available. It is usually divided into three steps: the measurement of the residual stress field in a certain area of the sample; the calculation of the eigenstrain values and the application of the eigenstrain to the same sample in order to know its entire residual stress field. The latter procedure is called Simple Triangle (SIMTRI) method. Although the method showed its versatility in different fields, the calculation of the eigenstrain is strictly dependent on the researcher's experience in making the correct choice of the polynomial fit used to predict the eigenstrain distribution and/or, as in the case of Achintha *et al*., high confidence is required in the ability of the FE modelling of the LSP simulation to obtain a correct set of eigenstrain values. Whilst we agree that the derivation of eigenstrain from experimental residual stress data is indeed indirect, it is nonetheless more physically accurate than that extracted from an FE model that may not accurately reproduce either the residual stress or the plastic strain field that led to it. A further different approach was published by DeWald *et al.* [21]. The method was applied to four samples of four different basic geometries and it is not based on the eigenstrain derived from the FE modelling of LSP but the eigenstrain are calculated from an RS field previously measured on a real sample.

Our goal in this paper is to apply the eigenstrain approach proposed by DeWald & Hill to an entire sample where different geometries are present at the same time in order to verify the independency of the eigenstrain from both the thickness and the geometry as was previously verified by Korsunsky with a different approach.

The eigenstrain approach proposed by DeWald & Hill consists of three different steps: first, a stress-free simple geometry sample (Fig. 1a) is laser peened over the entire surface. The residual stress measured as a function of position along the y direction (σ_{TOT}) can be seen as the superposition of two different components: the laser-peening-induced residual stress field (σ_{LP}); and the balancing elastic stress field generated by the material to balance the externally-induced component, formally called the equilibrium residual stress (σ_{EQ}). The total residual stress field is the summation of these two components. The first term, σ_{LP}, depends only on the LSP parameters [22] and is geometry-independent [11]; while the latter is dependent on the geometry of the peened component. This can be expressed as in Eq. 1:

$$\sigma_{TOT_{zz}}(y) = \sigma_{LP_{zz}}(y) + \sigma_{EQ_{zz}}(y)$$

Eq. 1. Superposition of laser-peen-induced (LP) and equilibrating (EQ) stresses

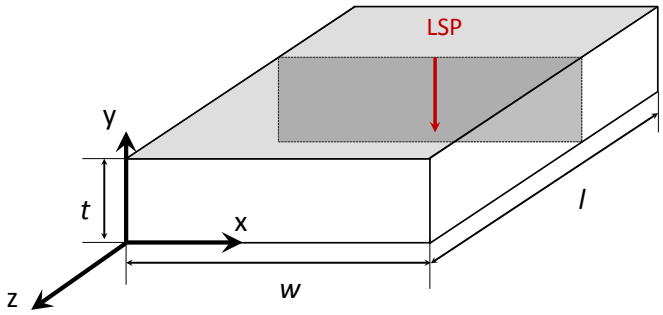

a)

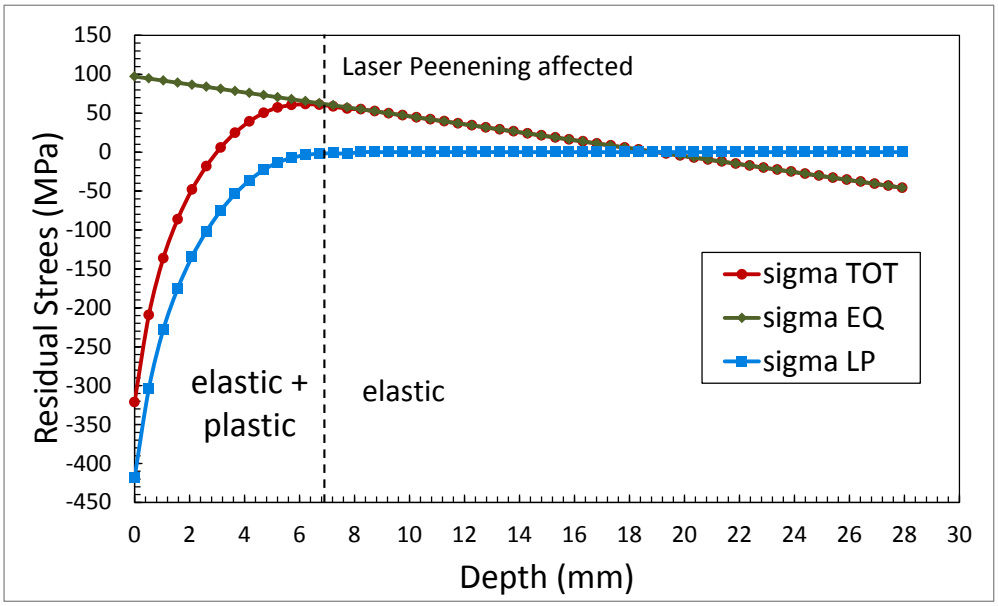

b)

Fig. 1 a) a simple geometry sample, peened on the top surface; b) separation of the stress components

Since the residual stress profile through the entire thickness is needed, the components of the stress must typically be measured either with the contour method or with neutron diffraction [23]. The equilibrium stress can be identified beyond the LSP-affected depth as an elastic balancing field as can be seen in Fig. 1 b). Achintha [19] measured the plasticity depth in an aluminium sample after LSP treatment using the full-width-half-maximum (FWHM) technique, confirming the higher dislocation density within the LSP-affected depth. By extrapolating the equilibrium stress component first and then by rearranging Eq. 1, it is possible to calculate the LSP stress component.

As reported in [21], since eigenstrains can be considered as an elastic strain distribution that produces the post-process residual stress field, we can easily calculate them from σ_{LP} using the following linear system:

$$\underline{\varepsilon^*}_{LP_{xx}}(y) = \begin{Bmatrix} \varepsilon^*_{LP_{xx}}(y) \\ \varepsilon^*_{LP_{yy}}(y) \\ \varepsilon^*_{LP_{zz}}(y) \end{Bmatrix} = -\frac{1}{E}\begin{bmatrix} 1 & -\nu & -\nu \\ -\nu & 1 & -\nu \\ -\nu & -\nu & 1 \end{bmatrix}\begin{Bmatrix} \sigma_{LP}(y) \\ 0 \\ \sigma_{LP}(y) \end{Bmatrix}$$

Eq. 2. Linear equations to calculate the eigenstrain values

We obtain three eigenstrain components for each depth location (according to the coordinate system in Fig. 1 a). By introducing the eigenstrain into the FE model of the sample and by solving for equilibrium, the model will generate a residual stress field. The process of introducing the eigenstrain inside the FE model imposes that every eigenstrain is introduced in the new FE model at exactly the same distance from the surface it was taken from. This is because the plasticity distribution must be the same in the two models: the one that the eigenstrains were calculated from and the new model used to predict the residual stress profile. The process is described more in detail in section 2.2.2 and was named by Korsunsky as the Principle of Transferability of Eigenstrain [18].

2 Materials

2.1 Sample

The sample studied is a stepped coupon made of aluminium alloy AA7050-T7451, milled from a rolled plate by EADS Innovation Works for fatigue testing with a Young's modulus of 72 GPa and a Poisson's ratio of 0.33. The material composition is listed in Table 1.

Element	Al	Cu	Mg	Zn	Zr
Weight %	89.0	2.3	2.3	6.2	0.12

Table 1 AA7050-T7451 composition

The sample is shown in Fig. 2. A complete description of all the samples involved in the broader research programme can be found in [5]. Two samples with the same geometry were laser shock peened by Metal Improvement Company (MIC), Earby, UK, with the same laser parameters but different patterns: the first one was laser peened over the upper face including the blend curved area and the lateral side as shown in Fig. 2, while the second sample was not peened on the lateral side; Fig. 3 shows the laser pattern used for this second sample. The following laser parameters were chosen to keep the distortions as low as possible: the power density was 4GW/cm^2; the duration of each shot was 18ns; and three successive layers of treatment were done with a 33% geometrical shift from each other. This level of coverage was expected to produce a homogeneous distribution of residual stress at the surface of the sample: low levels of coverage have previously been shown to introduce oscillatory stress fields [3]. The laser used a square spot size of 4 × 4 mm^2. The LSP process generated a maximum deflection of 0.2 mm as measured by [24] and was not taken into account

during the simulation with the eigenstrain approach.

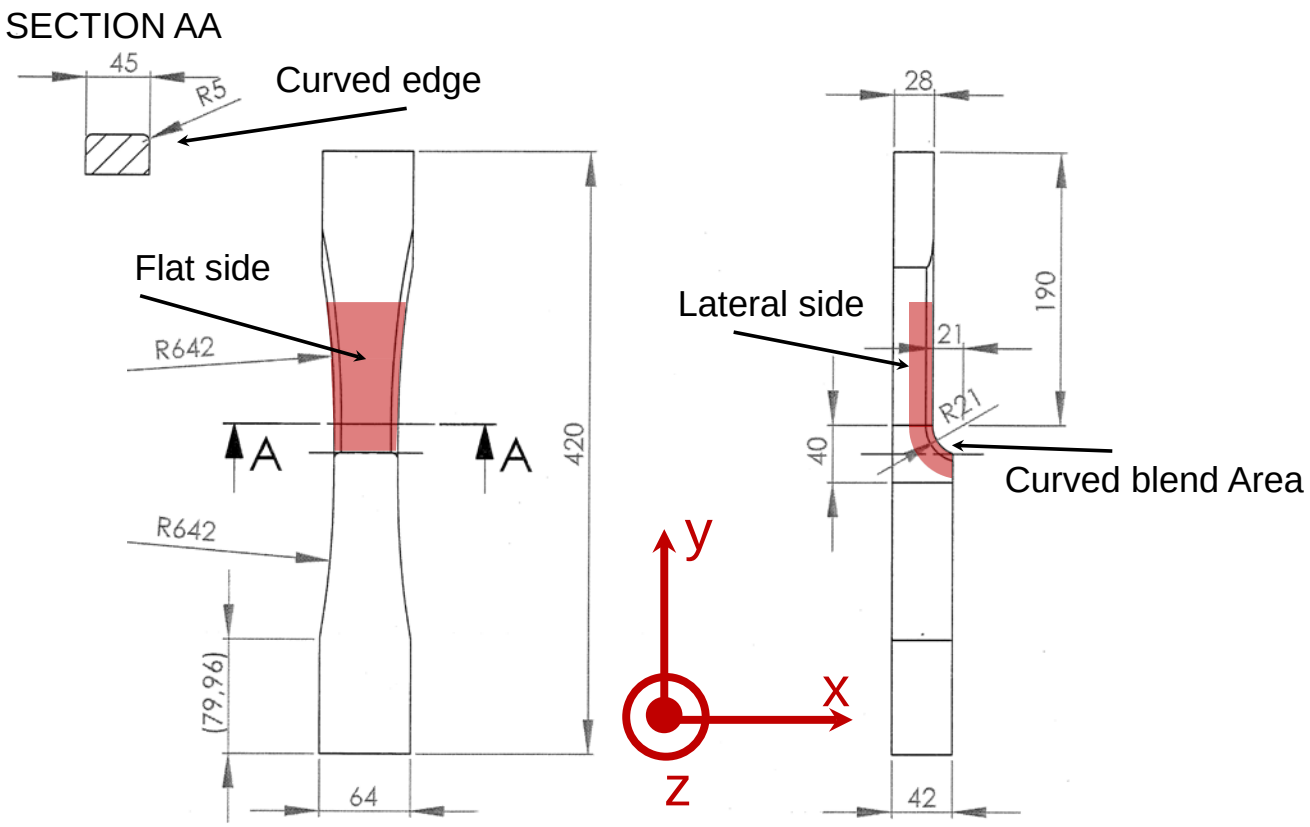

Fig. 2 The stepped coupon sample, with the axis system used and the area subject of this research. The red areas and the laser peened areas.

The sample provided three different areas for study: the central planar area from where the eigenstrains were derived; the curved edges at the extremes in the *y*-direction, where the effect of geometry change could be studied; and the curved blend between the two ends of the sample along the *x*-direction where the effect of thickness change could be studied.

Since the sample was to be subjected to neutron diffraction measurements, a microstructure analysis was carried out. As it is possible to see in Fig. 4, the coupon is textured in the z-direction which corresponds to the rolling direction of the original plate. Furthermore, a duplex grain structure is present. Grain size ranges from 2-3 μm up to 200 μm.

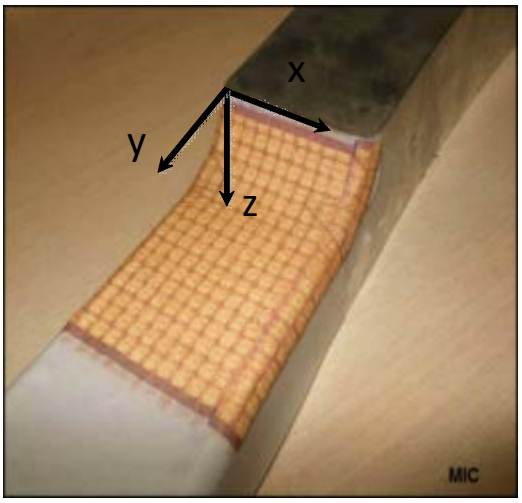

Fig. 3. Laser peening pattern: each square indicates the location of the laser shot.

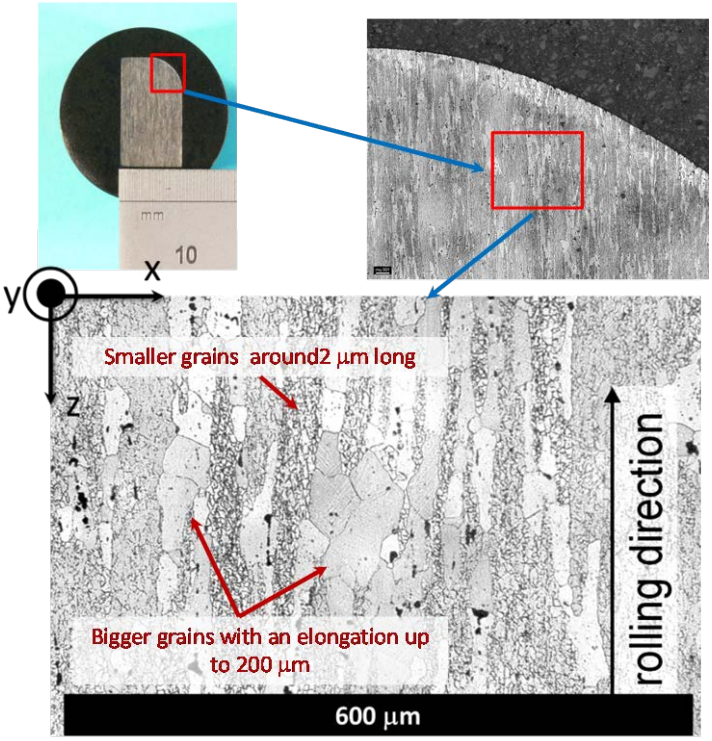

Fig. 4. Microstructure of the material measured at the curved edge. It is possible to see how the grains are elongated along the rolling direction.

3 Finite Element Analysis

3.1 Geometry

The sample was modelled with ABAQUS software [25]. Some changes were made from the real sample geometry to facilitate both the construction of the model and the application of the eigenstrains: while the forward part of the real sample is slightly divergent to assure a thinner section where the step is present, this divergence was not taken into account in the FE model since it would have complicated the modelling of the sample without bringing any benefit. Also, the material beyond the step was truncated since this material is present for clamping reasons only. The final model has 234,208 mesh elements.

3.2 Eigenstrain Application

Common methods to apply eigenstrains in an FE model are either to create several layers of materials which have the same elastic properties – same elastic modulus and same Poisson's ratio – but different thermal expansion coefficients; or to impose to each single node of the model the initial thermal strains: in the present study, the former option was chosen. As said before, eigenstrain can be seen as a mixture of inelastic strains of different origin, with no possibility to separate them into their single components. For this reason, modelling eigenstrain as thermal strains even if they are not actually of thermal origin will give the same result.

Based on the process to calculate the eigenstrain described in §1.1, the residual stress profile was measured in the middle section of the sample through the contour method. This method measures only one component of stress (σ_{yy} according to Fig. 6) but assuming that the LSP process generates a biaxial distribution of stress when applied over an area, the σ_{xx} component is considered to be the same as σ_{yy}, and σ_{zz} is considered to be 0 near the surface to meet plane stress criteria. Full details of the application of the contour method for this sample can be found in [24]. Once the entire profile of residual stress was obtained, it was smoothed in order to remove artefacts and noise in the data, as advised in [21]. The final smoothed residual stress profile was used as input in Eq. 2 to calculate the eigenstrain values. The smoothing process is concluded by polynomial fitting of the data to give the σ_{LP} profile as a function of the y coordinate. Data were extracted in 0.5 mm steps, thus, according to Eq. 2, every 0.5 mm we obtained three values of eigenstrain, one in each direction of the co-ordinate system.

The subsequent step regards the design of the FE model. Once the external geometry is set, as many sections as y positions have to be created in the same position where the eigenstrains are to replicate the plasticity behaviour of the LSP treatment. Each section has to be as thick as the step of the measurements. Once the different sections are created, the material of each section has to be assigned. Each material has to have two different properties: elastic and thermal. The elastic property is given by the Young's modulus (72 GPa) and the Poisson's ratio (0.33). The thermal properties are inserted in the model through the thermal expansion coefficients. The values of these coefficients are the eigenstrains calculated previously. It is worth noting that, since the thermal coefficient are not isotropic, a coordinate system has to be set for each area of interest. In particular as shown in Fig. 5, the material coordinate system at the round edge is inclined of 45° since the LSP treatment was done with the same inclination.

Fig. 5 shows the front section of the stepped coupon as was modelled for the FE analysis. This particular mesh was optimized for three different areas: the two rounded edges and the centreline of the sample. In these three areas, the different sections with different eigenstrains are 0.5 mm thick. Finally the sample was subjected a difference of 1˚ in temperature and solved for equilibrium.

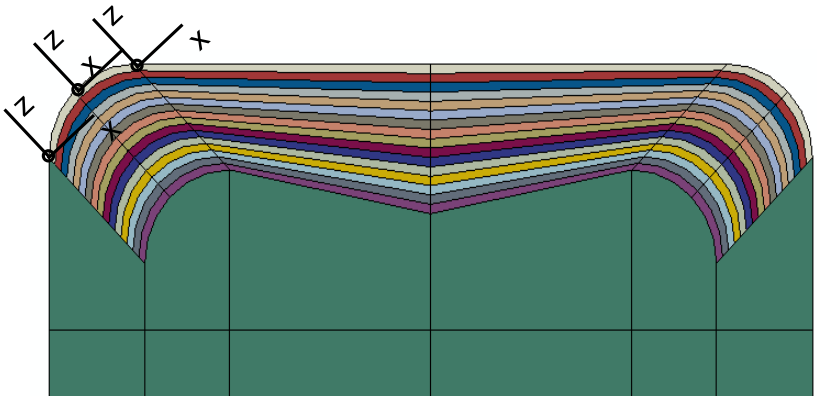

Fig. 1 FE model of the front section of laser shock peened sample. The area where eigenstrains were applied is clearly visible with different colours.

The different materials generate strains owing to the increment of temperature and, since the model is purely elastic, stress arises in the sample. The lack of clamping avoids any further generation of stress.

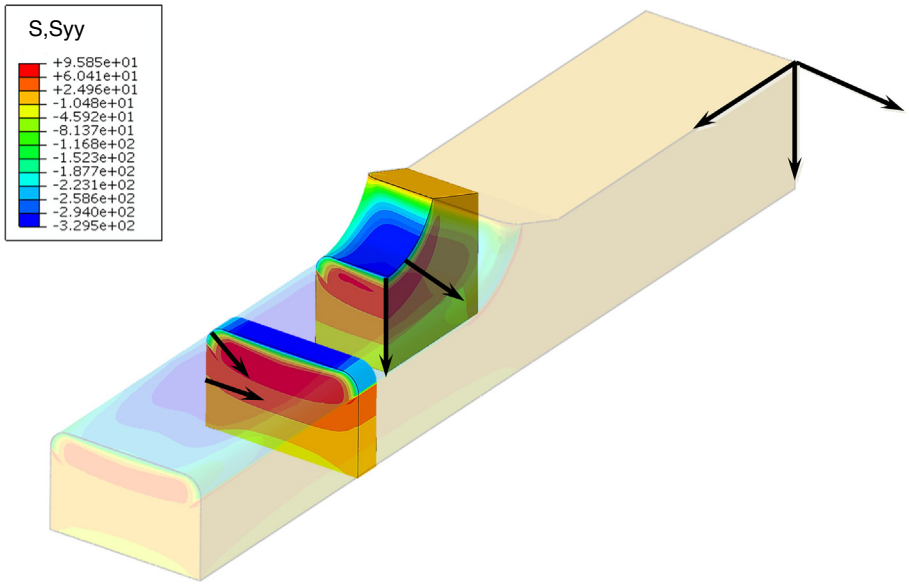

Fig. 2 The four arrows indicate the areas where comparisons between measured and eigenstrain-modelled data were made. From the top surface two different comparisons were made: in the plane area and the blended curve. On the lateral side two comparisons were made: one perpendicular to the lateral area and one at the curved edge (see Fig. 2 for clarification of the nomenclature).

4 Residual stress measurement methods

Three residual stress measurement techniques were applied. One sample was subjected to the contour method (1) to determine the S_{yy} stress component in the central area, Fig. 6. Then, since the contour method is a destructive method, a second sample was used to characterize the residual stress distribution in the curved area and at the round edge. In the first case, the neutron diffraction technique (2) was used while in the second both the contour method and incremental hole-drilling (3) were used to validate the data.

4.1 Contour Method

The contour method is a destructive residual stress measurement method introduced for the first time by Prime [26] in 2000 that is based on Bueckner's principle [27]. The process involves cutting the sample in the area of interest; subsequently, the relaxed surface profile is measured with a co-ordinate measuring machine (CMM) on both the surfaces of the cut. It has the advantage of providing a complete map of residual stress on the cut surface, but only one stress component can be obtained, which is the component normal to the cut surface. The data collected are first subjected to correction to remove any artefact coming from the cutting process, and are then smoothed. After averaging the data from both surfaces, they are imposed as negative displacements to an FE model. Assuming elastic relaxation of the surfaces, the displacements generate the residual stress distribution that was present before the cutting.

Diffraction techniques are non-destructive residual stress measurement methods which allow determination of a complete residual stress profile within certain limits. Diffraction techniques are based on Bragg's law, which states that particles are diffracted by the crystal lattice at an angle proportional to the relative distance between two atomic planes. By knowing this distance before any treatment (the so-called d_0 distance owing to the fact that the sample is assumed to be stress-free) and afterwards, it is possible to calculate the strains inside the sample and thence calculate the stresses.

4.2 Neutron Diffraction

The neutron diffraction technique [28,29] is mostly used when a deep penetration into the sample is needed since neutrons interact relatively weakly with matter which allows for a high penetration depth. The neutron beam is typically confined by apertures and/or collimators on the incident and diffracted beams to define the measurement gauge volume. When the gauge volume is immersed only partially in the sample, the disparity between the geometric centre of the gauge volume and the centre-of-gravity of the diffracting material generates fictitious strains formally called pseudo-strains. Several techniques can be used to prevent this error [30]. The one used during this study consisted of first measuring the residual stress values close to the surface with a partially-immersed gauge volume and then measuring the stress-free lattice parameter far from the stressed region with exactly the same partially-immersed gauge volume. During calculation of the strains, this value was used to calculate the effective strains close to the surface.

The measurements were performed at the Paul Scherrer Institute, Switzerland, which includes a spallation neutron source. The beamline used was POLDI (Pulse-OverLap DIffractometer), a time-of-flight thermal neutron diffractometer, dedicated to materials science applications [31,32]. During the measurements a gauge volume with a section of 2×2 mm^2 was used; the length of the gauge volume was set to 7 mm in the σ_{yy} direction (referring to the coordinate system in Fig. 5) both to decrease the amount of time per measurement and to include as many diffracting grains as possible to improve statistics.

4.3 Synchrotron X-ray diffraction

Synchrotron X-ray diffraction can provide fast measurements, even though the measurement depth is lower than neutron diffraction owing to the fact that X-rays have relatively low penetrability into metallic materials [33]. The gauge volume used with synchrotron X-rays is usually diamond-shaped with a small central width and a length that can be up to two orders of magnitude larger, depending on the diffraction angle. Pseudo-strains can again be detrimental for the measurements and this problem can be solved in the same way as for the neutron diffraction technique. Synchrotron X-ray diffraction was used in this experiment to measure the residual stress distribution from the lateral side of the sample, along the *y* direction according to the coordinate system in Fig. 2.

4.3.1 PETRA III

The first experiment was carried out at PETRA III in Hamburg (Germany), which is a monochromatic high-brilliance X-ray facility. The principal of Slit Imaging was used which consists of the determination of the strains based on the shift of the measured diffracted peak relative to the peak position of an unstressed sample [34]. At the beamline P07 [35] used for strain measurements a conical slit setup was available. The use of conical slits was first described in [36]: it consists of a plate with a series of concentric conical apertures that allows monitoring simultaneously a series of complete diffraction rings emanating from the same gauge volume. For every measurement, two components of strain are obtained. The potential of the conical slits to measure residual stress in laser shock peened samples was already demonstrated in [37]. For this experiment the energy was set to 74.5 keV in order to obtain a wavelength of 0.116 nm; with this set-up the strongest reflecting plane was {311}. The incoming beam had a cross-section of 50 × 50 μm^2, and the gauge volume length was approximately 1.2 mm.

The post-processing of the data was made through the FIT2D software provided by A. Hammersley at the European Synchrotron Radiation Facility. Since only one reflection plane was used to calculate the stress from the measured strains, a plane-specific Young's modulus should be used. However, Lorentzen reported in [38] that for the {311} reflection the Young's Modulus based on Kroner modelling scheme is equal to 70.2 GPa instead of 72 GPa measured with a tensile test. Since the difference is essentially around 2%, it can be considered negligible and a value of 72 GPa was kept for these calculations as well.

4.3.2 Diamond Light Source

A second experiment was carried out at the Diamond Light source (DLS), UK, using the beamline I12: Joint Engineering, Environmental, and Processing (JEEP) [39], a polychromatic X-Ray beamline. The experiment carried out at DLS aimed to measure the residual stresses at the curved edge. The gauge volume was diamond-shaped with a cross section of 50 × 50 μm^2, while the length was fixed at 2 mm. With this set-up, the closest measurement point to the surface was taken at 200 μm depth and measurements were taken up to 5 mm total depth. A "horseshoe" 23-element solid state detector is used at JEEP that allows simultaneous collection of strain measurements from 23 scattering vectors. The post-processing of

the data was carried out with DAWN software [40]. During the post-processing, only the {311} plane reflection was taken into consideration and the peak-fitting was made with a Gaussian curve.

4.4 Incremental hole-drilling

The conventional incremental hole-drilling method uses strain gauges to measure the strains that result from the redistribution of stresses around the drilled hole. In the system employed in this work, an Electronic Speckle Pattern Interferometer (ESPI) [41] replaces the strain gauges. This allows a fast, non-contact and easy measurement, avoiding the procedure of strain gauge application. In the case of a dull surface, no specific preparation of the sample is required for this technique. As it can be seen in Fig. 2, the sample surface was shiny. In order to avoid any reflection of the laser beam, the surface was first sprayed with an opaque paint and then was covered by paper tape leaving a small area where the measurements were performed.

The ESPI hole-drilling measurements were conducted at Helmholtz-Zentrum-Geesthacht, using a Stresstech PRISM system as shown in Fig. 7.

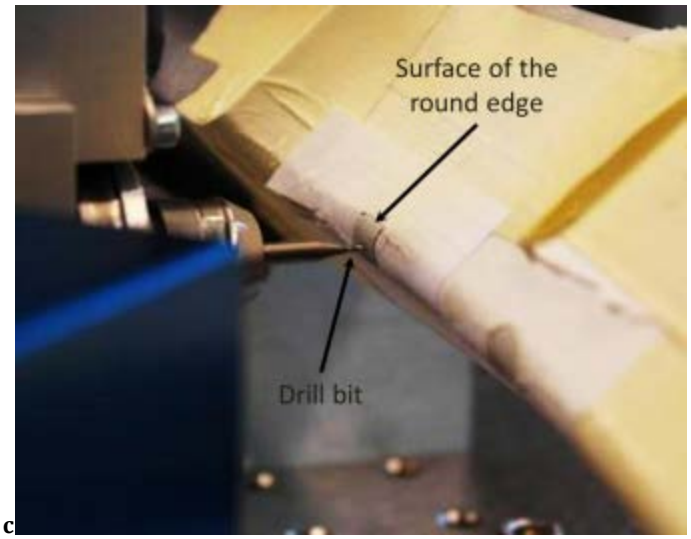

c

Fig. 3 Incremental hole drilling measurements

5 Results

5.1 Residual Stress in the Plane Area

An initial comparison was made between the measured residual stress in the central planar area and the residual stresses derived from the eigenstrain FE model. This gives verification that the eigenstrains were implemented correctly inside the ABAQUS environment, as they should reconstruct the measured residual stress. The measurements were taken from the planar area through the thickness, with the σ_{yy} component of stress obtained from the contour method. The residual stresses from the contour method at the planar area were compared with different techniques to increase the confidence, as shown in [42].It is possible to see, in Fig. 8, that the peak compressive and tensile stresses match extremely well, within an error of ±5

MPa that is within any technique sensitivity. The two curves should overlap perfectly in principle, since the eigenstrains were derived from the residual stress profile measured in the same position. However, there is smoothing applied to the data which accounts for the small differences observed between the two profiles. This first check confirmed the correct derivation of the eigenstrains and their application within the FE model.

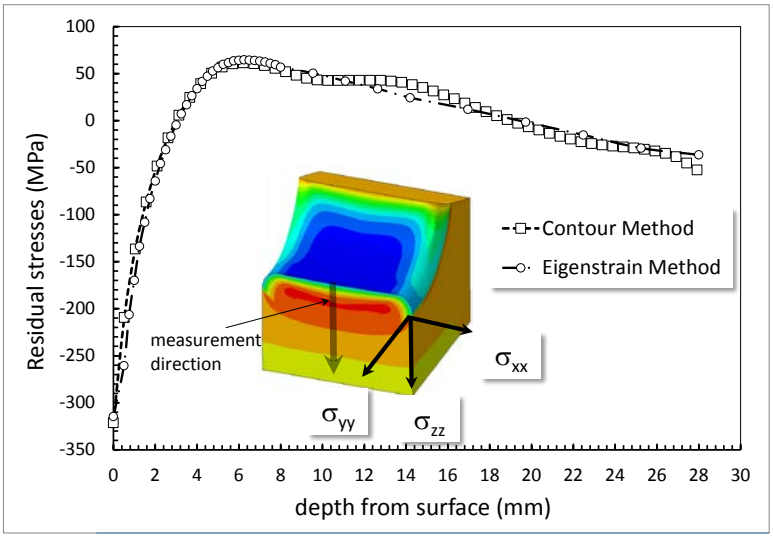

Fig. 1. Comparison between the Contour method results and the Eigenstrain approach results for the σ_{yy} residual stresses component.

5.2 Residual stresses at the Curved Edges

The derived eigenstrains were used to calculate the stresses normal to the curved edges of the sample. Fig. 9 shows the results of the eigenstrain calculation using the eigenstrains derived from the planar region of the sample, compared to the measured results from the contour method. There is a good agreement, within ±20MPa, from a depth of 1.5 mm from the surface. However, there is a significant discrepancy within the first 1.5 mm from the surface where the gap is up to 82 MPa: the compressive residual stress peak calculated with the contour method is at the surface and has a value of –154 MPa; the value predicted at the same position with the eigenstrain simulation is –236 MPa. A further residual stress measurement was carried out with the surface X-ray technique. The measured value at the surface of the round edge is –208±10 MPa.

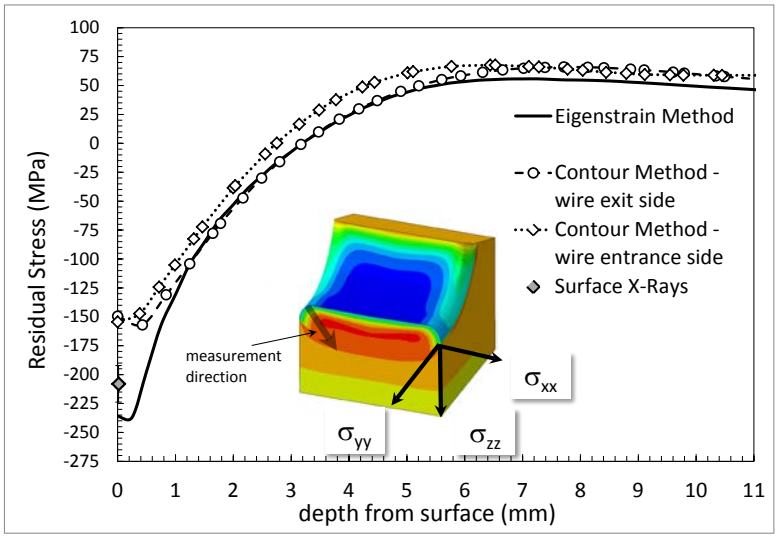

Fig. 2. Comparison between the Contour method results and the Eigenstrain approach results for the σ_{yy} residual stress component.

In order to have a further measurement set of data, the incremental hole-drilling technique was used for its higher reliability close to the surface. In Fig. 10 all these data are presented.

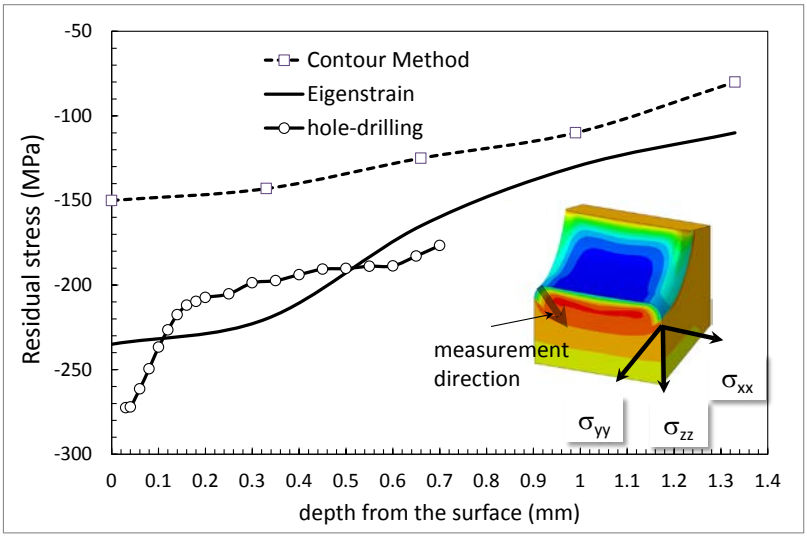

Fig. 3. Comparison between the Contour method results, the Eigenstrain approach results and the hole-drilling results for the σ_{yy} residual stress component.

Fig. 10 shows that the measurements taken at the round edge by incremental hole-drilling lay between the eigenstrain prediction and the contour method measurements between 0.1 mm and 0.7 mm depth, while between 0 and 0.1 mm the data were more compressive than either method. In particular, the measured value at the surface of the round edge is –275 MPa and the stresses reach a value of –210 MPa within the first 0.1 mm from the surface in depth. Between 0.1 and 0.7 mm from the surface in depth the values lie between –210 and –175 MPa.

Finally, a residual stress measurement on the same region was carried out at Diamond Light Source. The measurements were still made at the corner radius, from outside the sample up to 5 mm from the surface within the sample.

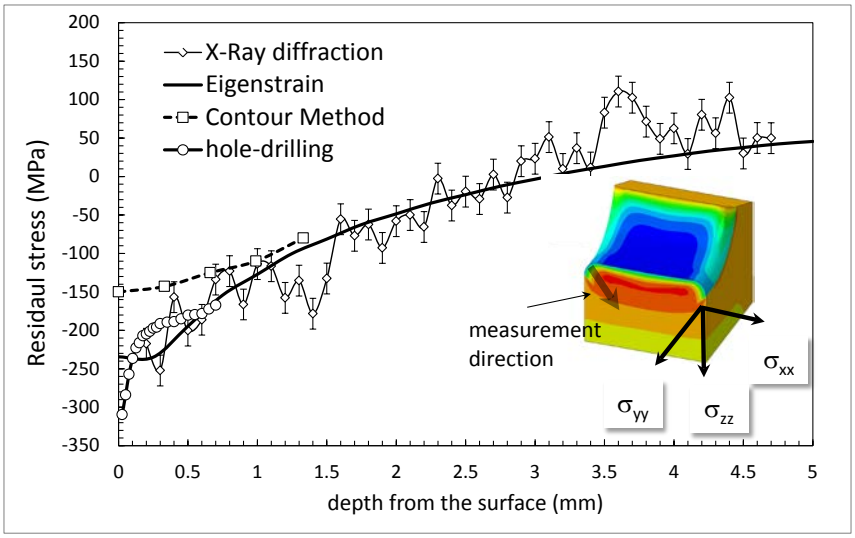

Fig. 4. Comparison between residual stress measurements along the direction indicated in the picture. The stress components is the σ_{yy}.

Fig. 11 shows the comparison between the eigenstrain prediction and the measured residual stresses in the σ_{yy} component along the direction indicated in the picture, with all the three techniques used. The agreement between the eigenstrain prediction and the synchrotron X-ray data is very good for the entire set of data from 0.2 mm from the surface up to 5 mm within the sample.

5.3 Curved blend area

An experiment was carried out with neutron diffraction using the POLDI (Pulse-OverLap DIffractometer) instrument at PSI, Switzerland [32]. The residual stress in the blend area between the ends of the sample was measured to investigate the applicability of the eigenstrain approach when the thickness is changed. Measurements were taken from the centre of the blend, normal to the sample surface. Fig. 12 b), c) and d) show the results for the three stress components according to the coordinate system shown in **Fig. 12** a):

a)

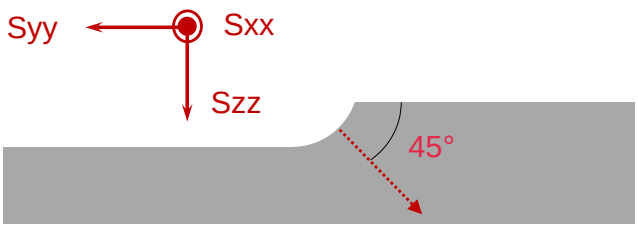

b)

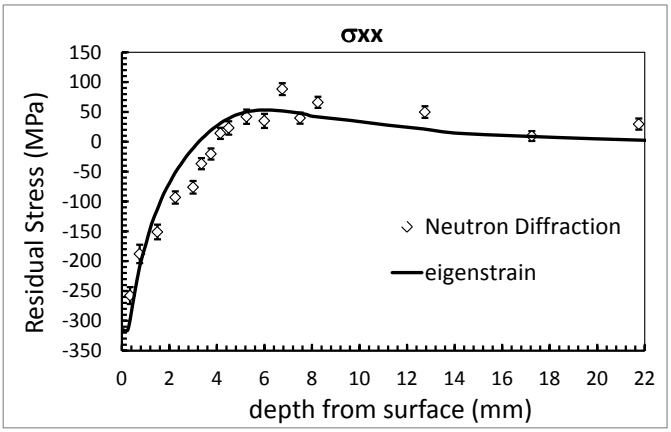

c) d)

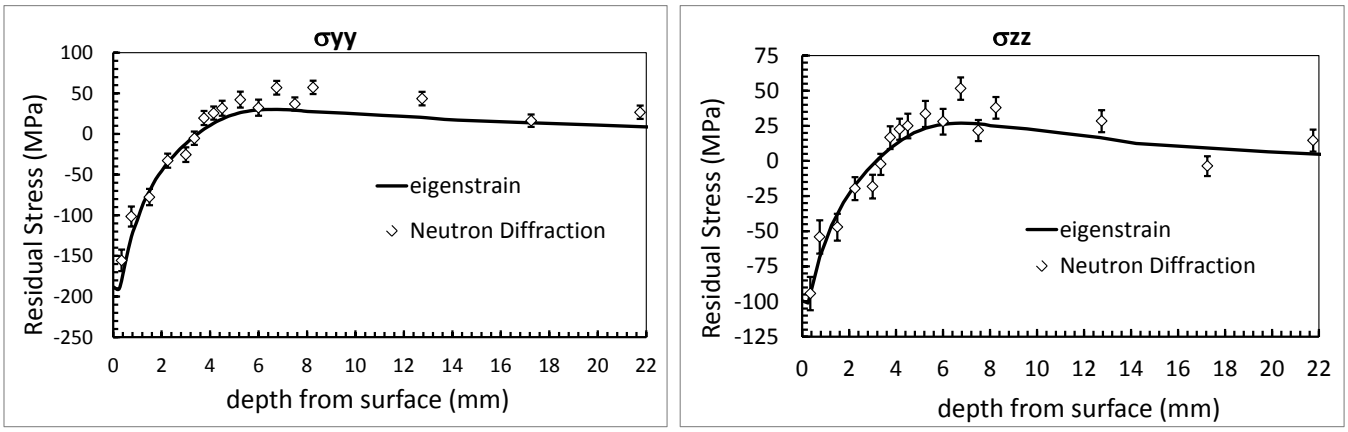

Fig. 1. a) Direction of the measurements and coordinate system; b) σ_{xx} stress component; c) σ_{yy} stress component; d) σ_{zz} stress component;

5.4 Lateral Side

The residual stress measurements from the surface of the lateral side (according to Fig. 2) along the y direction were made at the PETRA III synchrotron source, using the beamline P07 for strain measurement. A conical slit arrangement was used to reach a depth of 7 mm into the thickness. In Fig. 13 the comparison between the eigenstrain approach and the three measured stress components is shown:

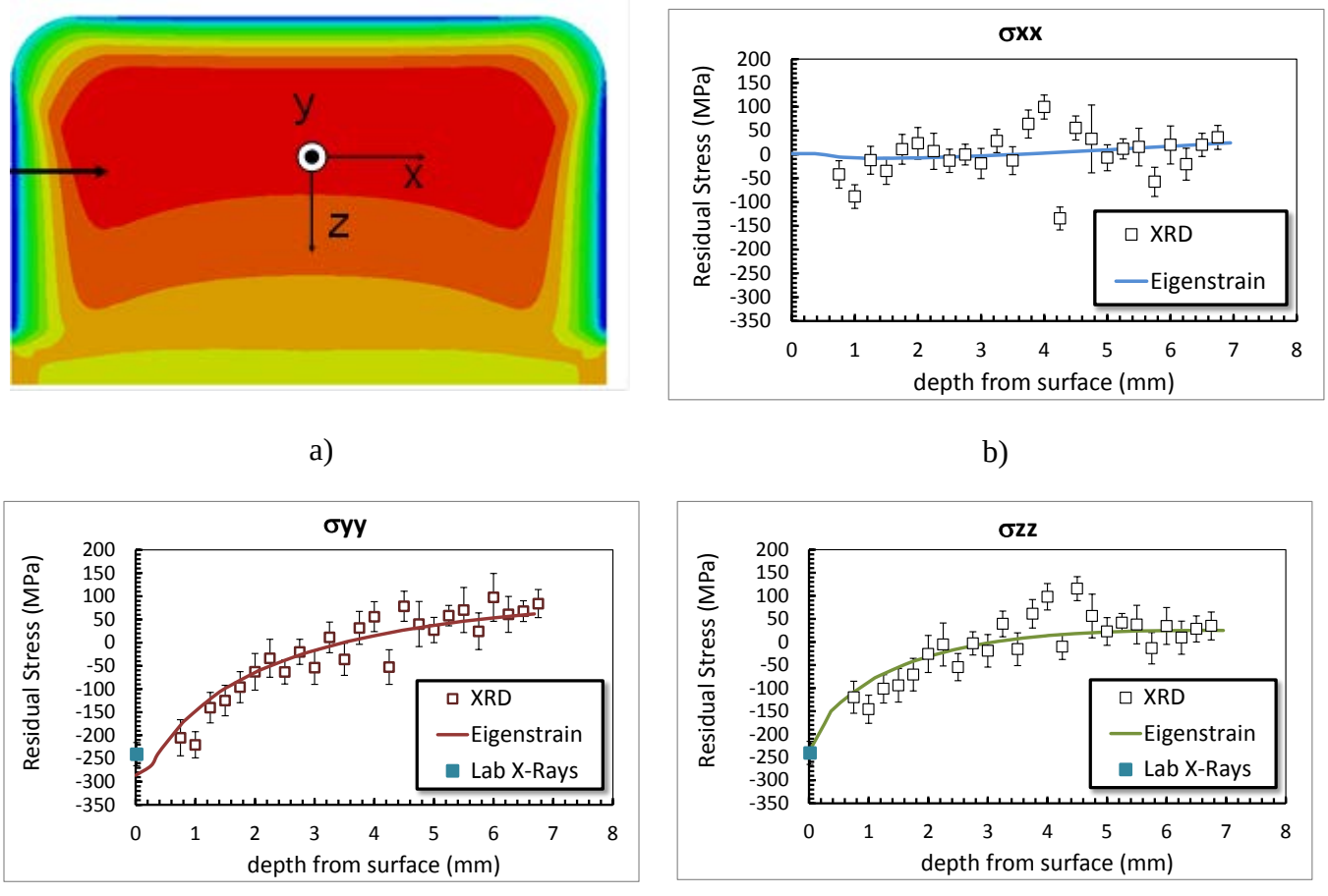

a) b)

c) d)

Fig. 1 comparisons between the eigenstrain distribution and the calculated stresses measured along the arrow showed in a) for the σ_{xx} component of stress b), σ_{yy} component of stress c) and σ_{zz} component of stress d).

6 Discussion

In this study the most challenging part was to accurately calculate the residual stress close to the surface of the round edge with a radius of 5 mm. The contour method was used first and it is well known that the technique is not reliable very close to a surface as a consequence of near-surface cutting artefacts and limitations in the data fitting [43]. Since it was impossible to establish *a priori* if either the contour method or eigenstrain approach were respectively underestimating or overestimating the residual stress values, the incremental hole-drilling technique was used for its higher reliability close to the surface. Two measurements were obtained at the curved edge to increase the reliability of the collected data, and we believe that this is the first time that incremental hole-drilling has been used to determine residual stress from a curved surface after LSP. The two residual stress profiles obtained were averaged. Generally speaking, the residual stress profile of laser shock peened component tends to vary smoothly very close to the surface and have the peak compressive stress below the surface owing to the reverse yielding effect. The ESPI hole-drilling technique suggests a residual stress profile that tends to be steeper close to the surface, which looks unrealistic. This apparent trend may be due to the fact that during the drilling the material very close to the surface was not removed homogeneously, so the data may not be completely reliable: and also some further limitations should to be taken into account with this technique such as the effects of surface roughness, drilling angle and determination of the surface location. Also, the system used performs simple drilling of the hole, and it is known that orbital milling produces more accurate results [44].

The analysis method of the deformed area around the hole using the ESPI technique requires certain assumptions. One of the assumptions is that the surface of the sample is flat before drilling the hole, out to at least about 5 diameters from the centre of the hole [45]. The ESPI measurement technique interprets the deformation as if the surface were flat. The present measurements did not account for the curved surface. This could be a further explanation to the steeper trend of the curve near the surface. In consequence, the results from the hole-drilling are not reliable near the surface, but can be taken to be acceptable after 0.1 mm depth; and since these data are closer to the eigenstrain approach than to the contour method (with a gap of 10 MPa only), this may indicate that the peak magnitude of near-surface compression was not adequately captured by the original contour method measurements from the central planar area. The difference may alternatively be a consequence of a change in material response to the peening at the curved edge. The laser spot was 4 × 4 mm^2 which is of the same order as the radius of the curved edge. This may have led to a different generation of shock waves and their interaction within the sample, and consequently a different distribution of residual stresses. Both surface and synchrotron X-rays were used in order to improve the knowledge of the residual stress distribution close to the surface and within the thickness. The surface X-ray measured data is very close to the eigenstrain-based prediction even though it

is worth noting that the surface X-ray with a Cr-α tube measures at the depth of 17 μm from the surface in aluminium alloys [46]. Synchrotron X-ray data show a good match with the prediction data for the entire profile from 0.2 mm for the surface up to 5 mm from the surface in depth. Since the diamond-shaped gauge volume was very narrow and elongated, where large grains were present inside the sample, data scatter is more evident. This is particularly noticeable around 1.5 mm from the surface and 3.7 mm from the surface. Regarding the blended curved area, Fig. 12 shows that the agreement between the eigenstrain prediction and the data from POLDI are within the measurements' error band for most of the points in directions σ_{yy} and σ_{zz}. For the σ_{xx} component there are some differences between the neutron measurements and the data from the eigenstrain prediction at around 2-5 mm depth. Close to the surface some pseudo-strains corrections were made as described previously in this paper, and the corrected results match the eigenstrain predictions within the error band. Owing to the large dimension of the gauge volume, more grains contributed to the diffraction process and the scattering was dramatically reduced.

Fig. 13 shows the residual stresses predicted with the eigenstrain approach where the sample thickness is much larger than the thickness form where the eigenstrains were derived. The predicted trend lies within the error bands of most of the measured data. A further data point was measured at the surface of the curved edge with surface X-Ray diffraction. Only σ_{yy} and σ_{zz} components were measured since the σ_{xx} can be considered zero by invoking plane stress. The surface XRD data also show good agreement with the eigenstrain approach, increasing confidence in its reliability.

The data from within the first 0.5 mm from the surface were removed because they were affected by pseudo-strains and no corrections could be made. The unstressed lattice parameter was measured for the σ_{yy} and σ_{zz} component only, owing to time constraints. The d_0 value for the σ_{zz} components was calculated based on the fact that the σ_{zz} components must be 0 at the surface. Furthermore, it is possible to see that at 4.5 mm depth there is some scattering in the measured residual stresses. This could derive from the presence of a large grain or grains which occupied a large portion of the gauge volume.

7 Conclusions

In this study the application of the eigenstrain theory was investigated on a laser-shock-peened aluminium alloy sample containing changes in geometry. Laser peening was applied to a flat, planar surface, and to curved surfaces with both convex and concave radii, and the possibility to predict the residual stress profiles generated by the LSP surface technique by the eigenstrain method was validated by a combination of the contour method, neutron diffraction, synchrotron X-ray diffraction and incremental hole-drilling. Eigenstrains for the plasticity induced by the laser peening were calculated from the planar section of the sample. The following conclusions can be highlighted:

1. As expected, introducing the eigenstrains into an FE model accurately re-created the original residual stress field.

2. Where the thickness of the sample increased, on the concave surface with low curvature radius compared to the laser peen spot size, the eigenstrain approach accurately predicts the trend of the residual stress profile in the three components of the stress, demonstrating that the eigenstrain are thickness-independent within the range of thickness studied.

3. Where the geometry changed significantly relative to the planar section, on the convex curved edges of the sample, the eigenstrain theory shows discrepancies relative to the experimental measurements. Some of the discrepancies may arise from limitations of both the raw contour data used to calculate the eigenstrain field, as the contour method has various sources of inaccuracy when determining near-surface residual stress; and the ESPI technique within the first 0.1 mm from the surface in depth due to the non-uniform drilling process at the surface. This highlights a limitation of the method in cases where there is low confidence in the baseline experimental data.

4. Owing to its higher spatial resolution, the synchrotron X-ray technique showed a trend closer to the eigenstrain prediction up to 0.2 mm from the surface in depth. This might due to the higher reliability of this technique close to the surface compared with the one obtainable with the contour method and ESPI.

We summarise that the eigenstrain theory is a conceptually-simple and time-efficient approach for the prediction of residual stress. However, attention has to be paid in the derivation of the eigenstrains, and caution taken if the geometry of the sample changes significantly from that from which the eigenstrains are derived. DeWald's approach has demonstrated its versatility even when the eigenstrains are used to predict the residual stress field in sections of increased thickness or non-flat geometries such as convex and concave radii.

Acknowledgments

The authors would like to thank Dr S. Van Petegem, beamline scientist at POLDI instrument, for his constant support during the experiment and data post-processing; Dr P. Staron and Dr T. Fischer for their support at beamline P07, PETRA III; and Dr M. Drakopoulos, Dr T. Connolley and Dr M. Hart for their support at the JEEP beamline, Diamond Light Source. MEF is grateful for funding from the Lloyd's Register Foundation, a charitable foundation helping to protect life and property by supporting engineering-related education, public engagement and the application of research.

References

[1] E. Maawad, Y. Sano, L. Wagner, H.-G. Brokmeier, C. Genzel, Investigation of laser shock peening effects on residual stress state and fatigue performance of titanium alloys, Mater. Sci. Eng. A. 536 (2012) 82–91. doi:10.1016/j.msea.2011.12.072.

[2] Y. Sano, M. Obata, T. Kubo, N. Mukai, M. Yoda, K. Masaki, et al., Retardation of crack initiation and growth in austenitic stainless steels by laser peening without protective coating, Mater. Sci. Eng. A. 417 (2006) 334–340. doi:http://dx.doi.org/10.1016/j.msea.2005.11.017.

[3] M. Dorman, N. Smyth, A. Cini, M.E. Fitzpatrick, P.E. Irving, M.B. Toparli, Effect of laser shock peening on residual stress and fatigue life of clad 2024 aluminium sheet containing scribe defects, Mater. Sci. Eng. A. 548 (2012) 142–151.

[4] H. Luong, M.R. Hill, The effects of laser peening and shot peening on high cycle fatigue in 7050-T7451 aluminum alloy, Mater. Sci. Eng. A. 527 (2010) 699–707. doi:http://dx.doi.org/10.1016/j.msea.2009.08.045.

[5] U.C. Heckenberger, V. Holzinger, W. von Bestenbostel, E. Hombergsmeier, Laser shock peening to improve the fatigue resistance of AA7050 components, Int. J. Struct. Integr. 2 (2011) 22–33.

[6] A.H. Clauer, S.C. Ford, C.T. Walters, The Effect of Laser Shock Processing on the Fatigue Properties of AA2024-T3 Aluminum, Lasers Mater. Process. 1983, Los Angeles, Calif. (1983).

[7] U. Trdan, S. Žagar, J. Grum, J.L. Ocan˜a, Surface modification of laser- and shot-peened 6082 aluminium alloy, Int. J. Struct. Integr. 2 (2011) 9–21. doi:10.1108/17579861111108572.

[8] W. Braisted, R. Brockman, Finite element simulation of laser shock peening, Int. J. Fatigue. 21 (1999) 719–724. doi:http://dx.doi.org/10.1016/S0142-1123(99)00035-3.

[9] J.L. Ocaña, C. Molpeceres, J.A. Porro, G. Gómez, M. Morales, Experimental assessment of the influence of irradiation parameters on surface deformation and residual stresses in laser shock processed metallic alloys, Appl. Surf. Sci. 238 (2004) 501–505. doi:10.1016/j.apsusc.2004.05.246.

[10] H.K. Amarchinta, K. Langer, D.S. Stargel, R. V. Grandhi, Material model validation fro laser shock peening process simulation, Model. Simul. Mater. Sci. Eng. 17 (2009).

[11] T. Mura, Micromechanics of Defects in Solids (Mechanics of Elastic and Inelastic Solids), Martinus Nijhoff Publiesher, 1987.

[12] T. Reissner, Eigenspannungen und Euigenpannungensquellen, J. Appl. Math. Mech. I (1931) 1–8.

[13] H. Murakawa, S. Rashed, S. Sato, D. Deng, Prediction of Distorsion Produced on Welded Structures during Assembly Using Deformation und Interface Element, J. Weld. Res. Inst. 38 (2009) 63–69.

[14] J.D. Eshelby, The Determination of the Elastic Field of an Ellipsoidal Inclusion, and Related Problems, Proc. R. Soc. London. Ser. A. Math. Phys. Sci. 241 (1957) 376–396. doi:10.1098/rspa.1957.0133.

[15] V. Luzin, Use of eigenstrain concept for residual stress analysis, in: Int. Conf. Residual Stress 9, Garmisch-Parterkirchen, 2012.

[16] Y. Nyashin, F. Ziegler, V. Lokhov, Decomposition method in linear elastic problems with eigenstrain, J. Appl. Math. Mech. 85 (2005) 557–570.

[17] H.T. Luckhoo, T.S. Jun, A.M. Korsunsky, Inverse eigenstrain analysis of residual stresses in friction stir welds, Procedia Eng. 1 (2009) 213–216. doi:10.1016/j.proeng.2009.06.050.

[18] A.M. Korsunsky, On the modelling of residual stresses due to surface peening using eigenstrain distributions, J. Strain Anal. 40 (2005) 817–824.

[19] M. Achintha, D. Nowell, K. Shapiro, P.J. Withers, Eigenstrain modelling of residual stress generated by arrays of laser shock peening shots and determination of the complete stress field using limited strain measurements, Surf. Coatings Technol. 216 (2013) 68–77. doi:http://dx.doi.org/10.1016/j.surfcoat.2012.11.027.

[20] A.M.K. Tea-Sung Jun, Evaluation of residual stresses and strains using the Eigenstrain Reconstruction Method, Int. J. Solids Struct. 47 (2010) 1678–1686.

[21] A.T. DeWald, M.R. Hill, Eigenstrain-based model for prediction of laser peening residual stresses in arbitrary three-dimensional bodies. Part 2: model verification, J. Strain Anal. 44 (2008).

[22] R. Fabbro, P. Peyre, L. Berthe, X. Scherpereel, Physics and applications of laser-shock processing, J. Laser Appl. 10 (1998) 265–279. doi:doi:http://dx.doi.org/10.2351/1.521861.

[23] M. Prime, A.T. DeWald, Practical Residual Stress Measurement Methods, WILEY, 2013.

[24] M.B. Toparli, Analysis of Residual Stress Fields in Aerospace Materials After Laser Peening, The Open University, 2012.

[25] ABAQUS, ABAQUS 6.10 Analysis User's Manual, ABAQUS/Standard Doc. Version 6.10.2. (2010).

[26] A.R. Gonzales, M.B. Prime, The Contour Method: Simple 2-D Mapping of Residual Stresses, in: 6th Int. Conf. Residual Stress., Oxford, UK, 2000: pp. 617–624.

[27] H. Bueckner, The propagation of cracks and the energy of elastic deformation, Trans. Am. Soc. Mech. Eng. 80 (1958) 1225–1230.

[28] A.J. Allen, M.T. Hutchings, C.G. Windsor, C. Andreani, Neutron diffraction methods for the study of residual stress fields, Adv. Phys. 34 (1985) 445–473. doi:10.1080/00018738500101791.

[29] M.T. Hutchings, Neutron Diffraction Measurement Of Residual Stress Fields—The Answer To The Engineers' Prayer?, Nondestruct. Test. Eval. 5 (1990) 395–413. doi:10.1080/02780899008952981.

[30] L. Edwards, Near-surface stress measurement using neutron diffraction, in: A.L. M. E. Fitzpatrick (Ed.), Anal. Residual Stress by Diffr. Using Neutron Synchrotron Radiat., Taylor & Francis, London, 2003: pp. 233–248.

[31] U. Stuhr, Time-of-flight diffraction with multiple pulse overlap. Part I: The concept, Nucl. Instruments Methods Phys. Res. Sect. A Accel. Spectrometers, Detect. Assoc. Equip. 545 (2005) 319–329. doi:http://dx.doi.org/10.1016/j.nima.2005.01.320.

[32] U. Stuhr, H. Spitzer, J. Egger, A. Hofer, P. Rasmussen, D. Graf, et al., Time-of-flight diffraction with multiple frame overlap Part II: The strain scanner POLDI at PSI, Nucl. Instruments Methods Phys. Res. Sect. A Accel. Spectrometers, Detect. Assoc. Equip. 545 (2005) 330–338. doi:http://dx.doi.org/10.1016/j.nima.2005.01.321.

[33] M. Fitzpatrick, A. Lodini, Analysis of residual stress by diffraction using neutron and synchrotron radiation, Taylor & Francis, 2003.

[34] W. Reimers, A. Schreyer, H. Clemens, A.R. Pyzalla, Neutrons and Synchrotron Radiation in Engineering Materials Science, (2008) 177–194.

[35] N. Schell, A. King, F. Beckmann, T. Fischer, M. Müller, A. Schreyer, The High Energy Materials Science Beamline (HEMS) at PETRA III, Mater. Sci. Forum. 772 (2013) 57–61.

[36] S.F. Nielsen, A. Wolf, H.F. Poulsen, M. Ohler, U. Lienert, R.A. Owen, A conical slit for three-dimensional XRD mapping., J. Synchrotron Radiat. 7 (2000) 103–9. doi:10.1107/S0909049500000625.

[37] A.S. Gill, Z. Zhou, U. Lienert, J. Almer, D.F. Lahrman, S.R. Mannava, et al., High spatial resolution, high energy synchrotron x-ray diffraction characterization of residual strains and stresses in laser shock peened Inconel 718SPF alloy, J. Appl. Phys. 111 (2012) 84904–84912. http://dx.doi.org/10.1063/1.3702890.

[38] T. Lorentzen, Anisotropy of lattice strain response, in: M. Fitzpatrick, A. Lodini (Eds.), Anal. Residual Stress by Diffr. Using Neutron Synchrotron Radiat., Taylor & Francis, 2003: pp. 114–130.

[39] M. Drakopoulos, Diamond Light Source, (2012). http://www.diamond.ac.uk/Beamlines/Engineering-and-Environment/I12.

[40] M. Gerring, DAWN Science, (2014). http://confluence.diamond.ac.uk/display/DAWN/DAWN+Science.

[41] G.S. Schajer, Advances in Hole-Drilling Residual Stress Measurements, Exp. Mech. 50 (2010) 159–168. doi:10.1007/s11340-009-9228-7.

[42] M.B. Toparli, M.E. Fitzpatrick, S. Gungor, Improvement of the Contour Method for Measurement of Near-Surface Residual Stresses from Laser Peening, Exp. Mech. 53 (2013) 1705–1718. doi:10.1007/s11340-013-9766-x.

[43] F. Hosseinzadeh, P.J. Bouchard, P. Ledgard, Controlling the Cut in Contour Residual Stress Measurements of Electron Beam Welded Ti-6Al-4VAlloy Plates, Exp. Mech. 53 (2012) 829–839.

[44] A. Nau, B. Scholtes, Evaluation of the High-Speed Drilling Technique for the Incremental Hole-Drilling Method, Exp. Mech. 53 (2013) 531–542.

[45] M. Steinzig, E. Ponslet, Residual stress measurement using the hole drilling method and laser speckle interferometry: Part I, Exp. Tech. 27 (2003) 43–46. doi:10.1111/j.1747-1567.2003.tb00114.x.

[46] M.E. Fitzpatrick, A.T. Fry, P. Holdway, F.A. Kandil, J. Shackleton, L. Suominen, Determination of residual stresses by X-ray diffraction, Meas. Good Pract. Guid. (2005).